Mapping Desert Shrub Rangeland Using Spectral Unmixing and Modeling Spectral Mixtures with TM Data

Youngsinn Sohn and Roger M. McCoy

Abstract

Spectral unmixing experiments were done to explore the applicability of linear unmixing models, especially the basic least-squares method for mapping sparse vegetation in rangeland. Some important theoretical and technical issues involved in physical inversion problems were addressed. Based on the field reference spectra of image components, a constrained least-squares method was applied to Landsat Thematic Mapper data over an area in Long Valley, Nevada to calculate vegetation abundance in a pixel.

A method for formulating a well-conditioned spectral mixture by calculating the cosine of the angles between the candidate surface components was presented. This method provides a way to measure the separability of candidate endmembers quantitatively and derive spectral endmembers objectively. The results of this study suggest that the ambiguity or uncertainty in physical inversion problems arises from the inability to provide a complete set of representative reference spectra and to formulate a well-conditioned spectral mixture, not from the least-squares method itself. Some of import implications of the study include the following: (1) the unmixing techniques can provide moderate estimates of vegetation fractions in arid rangeland, where vegetation is sparse, with TM data; and (2) the degree of spectral pureness of endmembers should be consistent between endmember spectra that are used for unmixing.

Introduction

A subpixel mixture problem is one of the unique characteristics of remotely sensed image data provided in digital format. When surface materials of interest are smaller than the spatial resolution of the sensor, the signal sensed at the sensor is a mixture of the reflected radiance of the target materials plus an atmospheric contribution. So the value of each pixel is the composite spectral signature of surface materials, such as soil, rock, vegetation, manmade materials, and shade plus atmospheric effects. The interpretation of remotely sensed digital image data can be improved by an understanding of the spectral components within each pixel. This subpixel mixture problem of remotely sensed digital image data has been considered by several researchers (Pace and Detchmendy, 1973; Twomey, 1977; Adams *et al.*, 1986; Boardman, 1991; Shimabukuro and Smith, 1991; Roberts *et al.*, 1993). Although spectral inversion methods have been utilized for estimating subpixel components in various geologic applications and in mapping vegetation in arid rangeland, these techniques have not yet been fully recognized or rigorously tested in remote sensing fields. Even though physical inversion problems have been recognized as a valuable tool in many science and engineering fields, acquiring a reasonable solution to least-squares problems has been a difficult task. While introducing the mathematics of inversion to the remote sensing field, Twomey (1977) discussed the "fundamental ambiguity" involved in physical inversion problems. Twomey (1977) argued that most physical inversion problems are ambiguous because they do not have a unique solution; that the solution must be obtained by imposing constraints; that the reasonableness of imposed condition would dictate whether or not the unique solution is also reasonable; and that the ambiguity could only be removed if some grounds could be provided from outside the inversion problem.

Objectives and Methods

The objectives of this paper are (1) to address some of the theoretical and technical issues involved in physical inversion problems, especially constrained least-squares methods, and in the modeling of spectral mixtures; and (2) to explore the applicability of a linear unmixing model as a tool for mapping low density vegetation in a semiarid rangeland. First, we addressed the "fundamental ambiguity" problem involved in constrained least-squares methods. Then spectral unmixing experiments were done to test the applicability of the unmixing model for mapping sparse vegetation. Based on the field reference spectra of image components, a least-squares unmixing model introduced by Shimabukuro and Smith (1991) was applied to Landsat Thematic Mapper (TM) data over an area in Long Valley, Nevada to calculate vegetation abundance in a pixel. Field spectra were used for reference spectra because we were not able to find representative pixels for each candidate image component in the study area image. For modeling a mixture of components, the cosine of angles between candidate endmembers were calculated and compared to the signal-to-noise ratio of TM data. This study involves the following procedures:

- Reviewing the concepts of the basic least-squares methods and addressing the theoretical and technical issues involved,
- Measuring field spectra to acquire reference spectra,

Department of Geography, Geology & Anthropology, S 159, Indiana State University, Terre Haute, IN 47809.

Y. Sohn is presently with the ACT (Training and Research on the Human Dimensions of Global Environmental Change), University of Arizona, Tucson, AZ 85721 (sohn@castanha.act.arizona.edu).

R. McCoy is presently with the Department of Geography, O5H 270, University of Utah, Salt Lake City, UT 84112.

Photogrammetric Engineering & Remote Sensing, Vol. 63, No. 6, June 1997, pp. 707–716.

0099-1112/97/6306-707$3.00/0

- Calibrating TM and field spectra data,
- Modeling a spectral mixture of image component, and
- Unmixing.

Field spectra of the study area scene components were measured using the SE590 field spectrometer and were calibrated to the reflectance. The reflectance data were then convolved with the four TM bandpass transmission spectra (bands 1,2,3,4) to obtain reference spectra for spectral unmixing. Only four TM bands were used because the SE590 spectrometer does not cover the whole TM wavelength ranges. The SE590 spectrometer covers the 0.4 to 1.1μm wavelength ranges in 252 channels and the TM sensor covers the 0.45 to 2.35μm wavelength ranges in six channels. Field spectra were taken from 2 to 7 August 1993. The TM image scene used in this study was obtained on 16 August 1989 (Landsat 4, Path 40, Row 32, scene ID Y4258817540X0). Precipitation pattern and any activities that might cause changes in vegetation vigor, biomass, and surface parameters in the study area were checked. There were no significant changes in precipitation pattern in the study area during the time period, especially several months before image data acquisition and filed data collection. No other disturbances that might cause interannual variation in vegetation vigor and surface condition were found. The digital numbers of TM image data were converted to ground reflectance using the formulation presented in Markham and Barker (1985).

Linear Spectral Unmixing

Information extraction from remotely sensed digital image data using unmixing methods involves three steps. The first step is understanding the relationship between observed radiance and surface reflectance and the sensor mechanism. Understanding the parameters controlling surface reflectance and the relationship between the observed radiance and surface reflectance is important for calibrating image data and defining a spectral mixture. The next step is modeling the spectral mixture. The number of complete and separable image components, or endmembers in the mixture, should be defined. Finally, the model must be inverted for decomposition into fractions of image endmembers (Roberts, 1991). In many related studies, these necessary steps have not been fully considered. The modeling of spectral mixtures and the procedures for choosing endmembers appear arbitrary.

Most related studies have modeled the remotely sensed signature as a linear combination of major surface components or spectral endmembers, and applied the least-squares approach to decompose the observed signature into component mixtures. The objective of the least-squares method is to estimate the proportion of each component in an image pixel by minimizing the sum of squares of the errors. Several different methods have been employed for obtaining a least-squares solution. These methods can be grouped into three broad categories: (1) the basic least-squares method, which finds the closest point in a given subspace to a given point in function space (Shimabukuro and Smith, 1991; Boardman 1991); (2) Bayesian regression analysis, which assumes the normal distribution for data and noise (Pech *et al.*, 1986; Smith *et al.*, 1990; Roberts, 1991); and (3) factor analysis (Smith *et al.*, 1985; Heute, 1986). Because of its conceptual simplicity and elegancy, Shimabukuro and Smith's (1991) basic least-squares method was chosen, and the discussion will be focused on the basic least-squares method. This basic least-squares method does not require prior knowledge of cover composition for surface components or the assumption of data normality.

Linear Unmixing and the Least-Squares Method

A hypothesis of the linear spectral unmixing model is that the image spectra are the result of mixtures of surface materials and shade, and that each of these components is linearly independent of the other. The mixtures in the image are expressed as linear combinations of their respective spectra in the image. Spectral response of each image pixel in any set of spectral bands can be considered as a linear combination of the responses of each component that is assumed to be in the mixture (Shimabukuro and Smith, 1991). Thus, each pixel contains information about the proportion and spectral response of each component. Each pixel spectrum of a multispectral image can be modeled as a linear combination of a finite set of components. Given a linear system of m equations (bands) and n unknowns (components), a system of the form

$$\begin{aligned} a_{11}x_1 + a_{12}x_2 + \ldots + a_{1n}x_n + \varepsilon_i &= b_1 \\ a_{21}x_1 + a_{22}x_2 + \ldots + a_{2n}x_n + \varepsilon_i &= b_2 \\ &\vdots \\ a_{m1}x_1 + a_{m2}x_2 + \ldots + a_{mn}x_n + \varepsilon_i &= b_m \end{aligned} \quad (1)$$

or $\mathbf{Ax} = \mathbf{b}$ has a unique solution: i.e.,

$$\mathbf{x} = \mathbf{A}^{-1}\,\mathbf{b}, \quad (2)$$

when a system is exactly determined ($m = n$), where b_i is a spectral reflectance for the ith band of an image pixel containing one or more components, a_{ij} is a spectral reflectance of the jth component in the pixel for the ith spectral band, x_j is a fraction value of the jth component in the pixel, ε_i is an error term for ith spectral band, j is the number of components assumed to be in the mixture (1, 2, ..., n), and i is the number of spectral bands (1, 2, ..., m). When the number of equations and the number of unknowns are same ($m = n$), the coefficient matrix $\mathbf{A}$ is square. As long as a set of columns of $\mathbf{A}$ are linearly independent (rank ($\mathbf{A}$) = m), we find a vector $\mathbf{x}$ which belongs to one of the column spaces R^n ($\mathbf{x} \in R^n$) for which $\mathbf{Ax}$ *equals* $\mathbf{b}$ ($\mathbf{Ax} = \mathbf{b}$) by obtaining the inverse matrix of $\mathbf{A}$ in Equation 2.

If a system of equations involves more equations than unknowns ($m > n$) or involves fewer equations than unknowns ($m < n$), we cannot expect, in general, to find a vector $\mathbf{x}$ for which $\mathbf{Ax}$ *equals* $\mathbf{b}$ because the coefficient matrix $\mathbf{A}$ is rectangular. Instead, we are looking for a vector $\mathbf{x}$ for which $\mathbf{Ax}$ is *closest* to $\mathbf{b}$ ($\mathbf{Ax} \cong \mathbf{b}$). In this case, it is reasonable to choose $\mathbf{x}$ so as to minimize the average error in the m equations (Strang, 1980), and the least-squares problem arises. When a system of linear equation is overdetermined ($m > n$), to solve the problem $\mathbf{Ax} \cong \mathbf{b}$, we solve the normal equations

$$\mathbf{A}^{\mathrm{T}}\,\mathbf{Ax} = \mathbf{A}^{\mathrm{T}}\,\mathbf{b}. \quad (3)$$

The system of equations has a unique solution if the columns of A are linearly independent: i.e.,

$$\mathbf{x} = (\mathbf{A}^{\mathrm{T}}\,\mathbf{A})^{-1}\,\mathbf{A}^{\mathrm{T}}\,\mathbf{b}. \quad (4)$$

When a system of linear equations is underdetermined ($m < n$), the rank of ($\mathbf{A}$), r, is less than or equals m ($r \leq m$). If the system is inconsistent, there will be no solution. If the system is consistent, we can assign $n - r$ free variables arbitrary values and solve the problem $\mathbf{Ax} \cong \mathbf{b}$ to have an infinite number of solutions. As reviewed in this section, solving systems of linear algebraic equations involves finding the inverse of the coefficient matrix $\mathbf{A}$. The inverse matrix is a very important basic concept for solving the least-squares problems even though most of the practical methods for computing the solution of $\mathbf{Ax} \cong \mathbf{b}$ do not involve explicit computation of an inverse matrix, $\mathbf{A}^{-1}$.

Constrained Least-Squares Methods

Often, the general solutions obtained by inversion methods are mathematically acceptable but are physically unacceptable. For example, a minus value may best fit in mathematically but the fractions of surface components should be positive and sum up to unity. In most of the practical applications of the inversion methods for solving the problem $\mathbf{Ax} \cong \mathbf{b}$, the additional boundary conditions, i.e., linear constraints, are imposed to obtain a physically meaningful solution. Scientists in specific fields have developed techniques for the constrained least-squares problems of their own discipline. The linear spectral unmixing model in remotely sensed digital image analysis is one of the examples.

Shimabukuro and Smith (1991) modeled a TM image pixel as a linear combination of a finite set of components (Equation 1). Linear constraints are added: i.e.,

$$\sum_{i=1}^{n} x_i = 1 \quad \text{and} \quad x_i \geq 0 \quad \text{for all } i.$$

The linear model (Equation 1) can be rewritten in error terms: i.e.,

$$\varepsilon_i = b_i \sum_{j=1}^{n} (a_{ij} x_j). \tag{5}$$

The function to be minimized is

$$F = \sum_{i=1}^{m} \varepsilon_i^2 \tag{6}$$

For an $n = 3$ mixture model, by finding a minimum within the boundary, $0 \leq x_1 \leq 1$ and $0 \leq x_2 \leq 1$, Shimabukuro and Smith (1991) solved for x_1 and x_2. According to the outcomes of the unconstrained x_1 and x_2 values, x_1 and x_2 were recalculated if necessary. The values of x_3 were determined accordingly. Numerical methods for solving this problem are presented in Shimabukuro (1987) and Shimabukuro and Smith (1991).

Modeling a Spectral Mixture and Cosine of the Angles

Modeling of a spectral mixture using a certain number of spectral bands requires the testing of the orthogonality of column vectors in the matrix **A**. Suppose a linear system of m spectral bands in n components is modeled and any of the two components are a linearly scaled version of one another, i.e., they are linearly dependent and not orthogonal, then the system will fail to have a unique solution. If the system includes two components that are too close to one another to be independent, then the system is ill conditioned and estimates of the decomposition would not be reliable. Considering an $m \times n$ matrix **A** and, the vector space R^n consists of all column vectors with n components. A pseudo inverse, or a solution to the least-squares problem, exists only when the rank r is as large as possible, i.e., when $r = m$ or $r = n$ because an $m \times n$ matrix cannot have more than m independent rows or n independent columns. The rank r is the number of independent rows or columns in the matrix **A**. In the case of $r = m$, $\mathbf{Ax} \cong \mathbf{b}$ always has a solution, and in the case of $r = n$, the solution, if it exists, is unique. If $m \times n$ matrix **A** has linearly independent columns, so that $r = n$, then $\mathbf{A}^T\mathbf{A}$ is a square, symmetric, and invertible matrix. Then the least-squares solution to a system $\mathbf{Ax} \cong \mathbf{b}$ of m equations in n unknowns satisfies the normal Equations 3 and the system has a unique solution given in Equation 4.

In the two-dimensional plane spanned by two column vectors $\mathbf{v}_1$ and $\mathbf{v}_2$, $\mathbf{v}_1$ is orthogonal to $\mathbf{v}_2$ when they form a right angle. The inner product of the column vectors $\mathbf{v}_1$ and $\mathbf{v}_2$, which is denoted by $\mathbf{v}_1^T\mathbf{v}_2$, in n space is zero only when the two vectors are orthogonal. If the nonzero vectors $\mathbf{v}_1$, ..., $\mathbf{v}_k$ are mutually orthogonal, then they are linearly independent and completely separable spectrally. On the other hand, if those vectors are extremely close to being linearly dependent, all the vectors are linearly scaled versions of each other and spectrally unseparable. Generally, real reference spectra of endmembers are intermediate to these two extreme cases (Boardman, 1989) and they are not orthogonal. Even though the given vectors $\mathbf{v}_1$ and $\mathbf{v}_2$ are not orthogonal, when solving the problems of least squares of solution to an overdetermined system, the solution to the problem automatically brings in orthogonality (Strang, 1980). Suppose we are given a point b in n-dimensional space, and we want to find its distance to the line in the direction of the vector $\mathbf{v}_1$. We are looking along that line for the point p closest to b. Then the line connecting b to p (the dotted line in Figure 1) is perpendicular to the original vector $\mathbf{v}_1$. This fact allows us to find the closest point p, and to compute its distance from b (Strang, 1980).

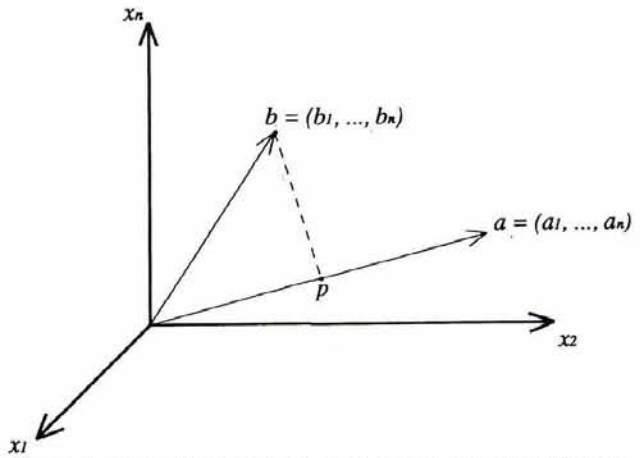

Figure 1. Projections in n-dimensional space. From Strang (1980), 2nd ed., copyright © 1980 by Harcourt Brace & Company.

With nonorthogonal vectors, the inner product of the two vectors gives a natural definition of the cosine of the angle between them in n space, and determines the angle between any two vectors. By measuring the cosine of the angles of the column vectors using this relationship of the inner product to the cosine of the angle in n space, we can decide if the column vectors are independent and spectrally separable in a system of m spectral bands in n unknowns. If the angle between the two vectors is larger than the signal-to-noise ratio, the two vectors are well differentiated. If the angle between the two vectors is smaller than the signal-to-noise ratio, then the noise would make it impossible to get a reliable decomposition, no matter how accurate the underlying model is. In Figure 2, for example, the vectors **a** and **b** are well differentiated because the angle between the two vectors, $\theta_{\mathbf{a},\mathbf{b}}$, is larger than the signal-to-noise ratio. However, the vectors **b** and **c** cannot be differentiated well because they are in the range of noise of one another.

The cosine of the angle between any two vectors $\mathbf{v}_1$ and $\mathbf{v}_2$ is

$$\cos\theta_{\mathbf{v}_1,\mathbf{v}_2} = \frac{\mathbf{v}_1^T\mathbf{v}_2}{\|\mathbf{v}_1\| \, \|\mathbf{v}_2\|} \tag{7}$$

where $\|\mathbf{v}_1\|$ and $\|\mathbf{v}_2\|$ are the lengths of vectors $\mathbf{v}_1$ and $\mathbf{v}_2$. The angle θ is defined by

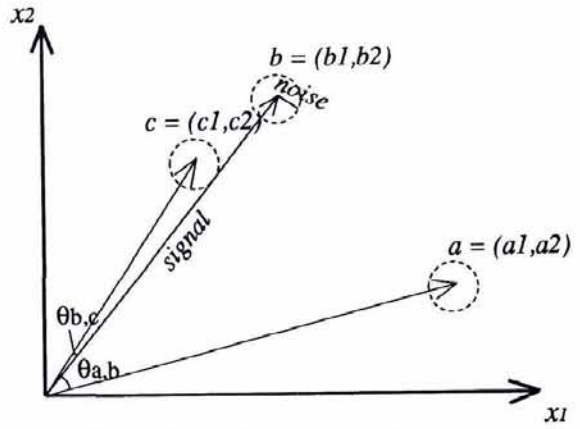

Figure 2. The angles and the separability between the vectors.

$$\theta = \cos^{-1}\left[\frac{\mathbf{v}_1^T\mathbf{v}_2}{\|\mathbf{v}_1\|\,\|\mathbf{v}_2\|}\right] \quad (8)$$

Equation 8 gives the difference in angle between the two vectors $\mathbf{v}_1$ and $\mathbf{v}_2$. The unit is radians with values ranging from zero to $\pi/2$.

Ambiguity and Constrained Least-Squares Methods

In their constrained least-squares method, Shimabukuro and Smith (1991) used an iterative method to obtain a solution. Starting with an unconstrained global minimum, if the minimum satisfies the boundary conditions, then it is the last solution. If the minimum does not satisfy the boundary conditions, the minimum is projected to a boundary and the problem is solved on this boundary. This is different from solving for the constrained minimum directly. It may look like Shimabukuro is steering to a solution by projecting the minimum to a boundary segment arbitrarily. Shimabukuro's method, however, is quite reasonable and safe for a quadratic function if the model is well conditioned. If the residual, ε, is a linear function of the parameters, then ε^2 is a quadratic function of parameters. If a function f (the function to be minimized in our case) is quadratic, then f will be quadratic along any linear parametized path through the domain. A one-dimensional quadratic function has only one local extrema, either a global minimum or a global maximum. So a one-dimensional quadratic function is monotonic on either side of its global extrema. It follows that, for a linear residual, the residual squared will increase monotonically along any line passing through the global minimum of the function f. Stated differently, the minimum of a function f in a region cannot occur at a point on the boundary of the region which is occluded from the global minimum of f by some other point on the boundary of the region. For example, in Figure 3a, the point p_2 cannot be the minimum of f over the region R. This means that, if the global minimum is outside the boundary, for example, somewhere in A in Figure 3b, we can unambiguously pick the boundary segment on which the constrained minimum occurs, that is, on the boundary a in Figure 3b. For well-conditioned systems, the chances of the global minimum being in one of these ambiguity regions are very small. Even if we end up in an ambiguity region and choose the wrong boundary segment once in awhile, the effect is small.

When a model is ill conditioned, that is, when two endmembers that are spectrally very close to one another are included together, a minimum can occur in the shaded region in Figure 3b. In this case, because it is not clear that point p is minimum of A or C, the decomposition would not be reliable. This is why it is important to measure spectral angles between the candidate endmembers for testing the separability of endmembers, and formulate a well conditioned model for unmixing. As long as the model is well conditioned, projecting a minimum occurring outside the boundary condition to a boundary, and solving the minimum on the boundary is very reasonable.

Study Area and Its Vegetation

The study area is located in the north-central part of Long Valley, White Pine County, Nevada (Figure 4a). The study area is roughly a 6.87- by 8.25-km area of the flat valley floor. Most parts of the valley average less than 2133 m above sea level, and the lowest part of the valley floor is about 1844 m above sea level. The valley lowland is underlain by valley fill deposits ranging in age from Tertiary to Quaternary. The valley fill includes unconsolidated gravel, sand, and clay deposited under subaerial and lacustrine conditions since the extrusion of the basalt flows. Only intermittent streams are found in the valley. Small springs in the

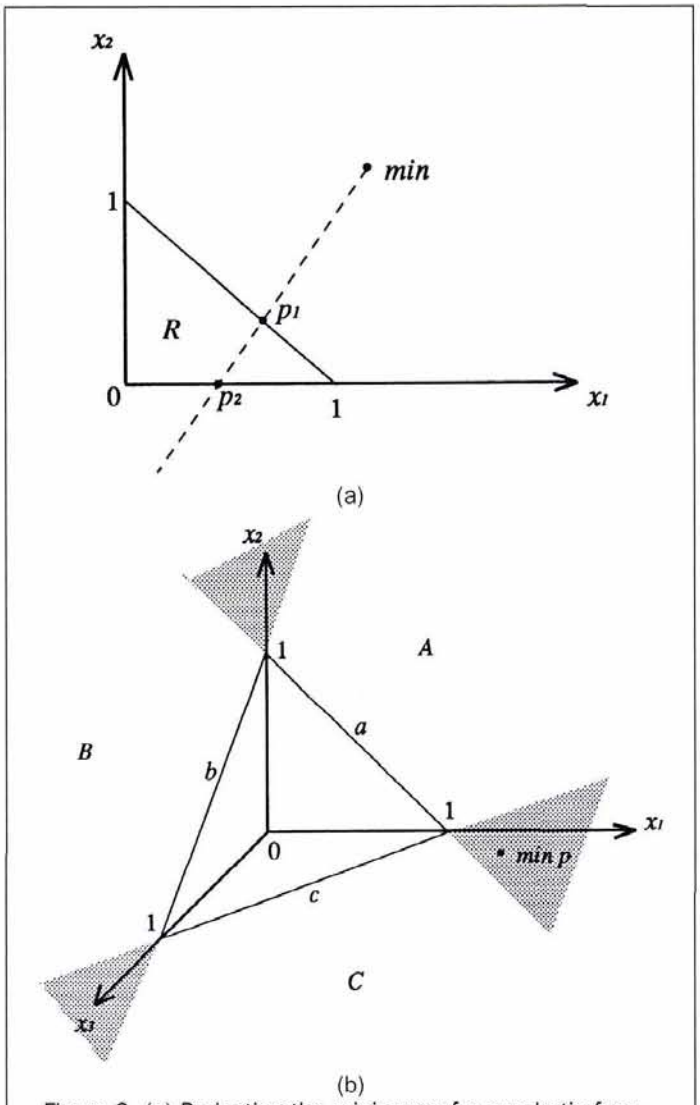

Figure 3. (a) Projecting the minimum of a quadratic function to a boundary. (b) The minimum occurring in an ambiguity region.

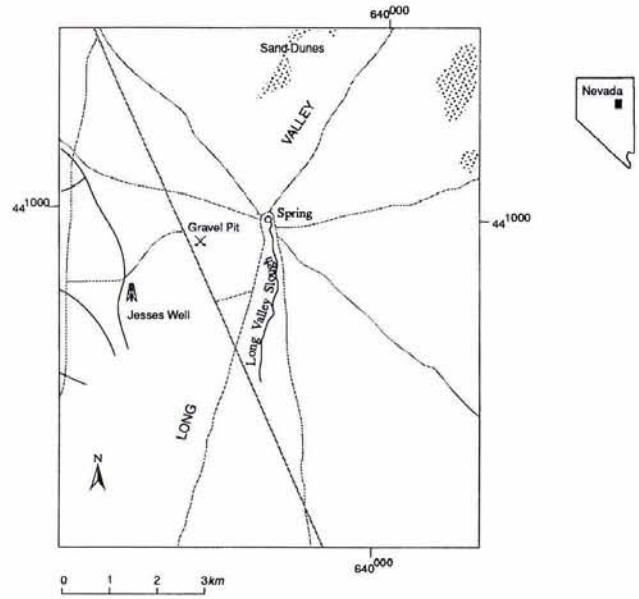

(a)

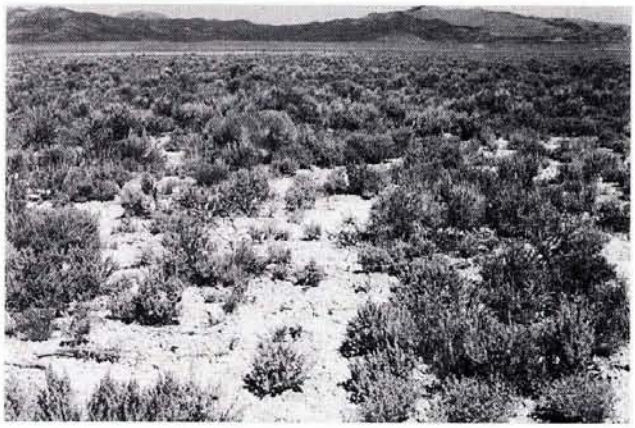

(b)

Figure 4. (a) Location of study area in Long Valley, Nevada. (b) The typical features of vegetation in the study area.

mountains, particularly in the south and west side of the valley, are supplied from perched ground water and used for livestock. The largest spring in the valley, Long Valley Slough, is found in the study area. In the Long Valley area, precipitation and humidity are generally low and summer temperatures and evaporation rates are high. Precipitation is very irregular and generally is least on the valley floors. The average annual precipitation between 1980 and 1992 in Ely, Nevada, the nearest town to the valley, ranges from 1,676 mm (1989) to 3,945 mm (1982). (Western Regional Climate Center, Reno, Nevada) The valley region showed a maximum temperature of 36.7°C in 1948, 1954, and 1959. The minimum temperature recorded was −36.7°C in 1949. Long Valley is used for livestock grazing, and several test wells were drilled for oil exploration. There is no other activity recorded in its past history (Eakin, 1961). There are no permanent residents or ranches in the valley.

Vegetation in the valley floor is characterized by a mixture of desert shrub dominated by big sagebrush (*Artemisia trinentata*) (Figure 4b). The big sagebrush is found at every sample site of the study area. Subdominant species are two types of rabbitbrush (*Chrysothamnus nauseosus* and *Chrysothamnus viscidiflorus*), greasewood (*Sarcobatus vermiculatus*), shadscale (*Atriplex confertifolia*), gardner saltbush (*Atriplex gardneri*), halogeton (*Halogeton glomerata*), and grasses such as squirreltail (*Sitanion hystrix*) and indian rice grass (*Oryzopsis hymenoides*). All the subdominant species are found only in limited areas. The measured maximum height of the shrub was 101.6 cm and the minimum height was 12.7 cm. The measured maximum canopy was 101.6 cm wide and the minimum canopy was 20.3 cm. Halogeton is found mostly in the distributed areas.

To gain insight into the study area for modeling a spectral mixture and to collect vegetation information, a field survey was done in October 1993. Forty-two sites were chosen for measuring the frequency of vegetation and the scene components in the study area. Each site was selected to represent different regions in the study area through unsupervised classification of the study area scene. Seven spectral clusters were generated for stratified random sampling. Through the preliminary field observation, we were convinced that seven clusters would cover all of the major variations in the study area. Dominant features of soil and vegetation for seven clusters are in Table 1. The clustered image was registered to UTM coordinates. For each cluster, five or six sites were selected. To avoid the boundary regions, each site was located near the center of a 20- by 20-pixel (at least) polygon of the same cluster. The UTM coordinates for each sample site were recorded from the screen. All the sample sites were located on 1:24,000-scale USGS topographic maps. At each site, two 30-m line transects were located. At 30-cm intervals along each of the transects, the observed ground cover materials were recorded. According to field estimates of percent cover, vegetation cover ranges from about 15 percent to 38 percent for each site. Through this field observation, dark and light color soils, green leaf vegetation (greasewood, shadscale, halogeton, rabbittbrush), gray and hairy leaf vegetation (sagebrush, saltbush), woody materials (dead stems), dry grass, and shade were identified as major surface components.

Unmixing in TM Data

Sampling and Measurement of Reference Spectra

Field spectra of candidate image components were measured using the SE590 field spectrometer from 2 to 8 August 1993.

TABLE 1. DOMINANT FEATURES OF SOIL AND VEGETATION FOR SEVEN CLUSTERS

Cluster	Dominant features of soil and vegetation
1	Small sagebrush with clumps of medium size sagebrush* Dark and bumpy soil with cryptograms and dark gravels**
2	Small sagebrush or shadscale mixed with dry grass, small rabbitbrush, or halogeton Dark and bumpy soil with cryptograms
3	A mixture of medium size sagebrush and rabbitbrush, Intermediate brightness soil
4	A mixture of big and medium size sagebrush and rabbitbrush or a mixture of sagebrush and greasewood Intermediate brightness and bumpy soil
5	A mixture of big and medium size sagebrush and greasewood Light and bumpy soil
6	A mixture of medium and small size sagebrush and greasewood Light and cracked soil
7	Small size saltbush or a mixture of small saltbush and small sagebrush, Very light and cracked soil

*small size: about 7 to 18 inches height, medium size: about 20 to 30 inches height, big size: about 30 to 40 inches height
**soil color and surface texture

To preserve the consistency and accuracy of field data, the general guidelines suggested by Milton (1987), McCoy *et al.* (1989), and Bammel and Birnie (1994) were followed. Out of 42 sample sites, 36 sample sites were chosen for field spectra measurement. Three of the sample sites were found inappropriate for collecting field spectra. Field spectra were measured from the resulting 33 sample sites. For each sample site, at least three spectral measurements were averaged for each major surface component, including soil and shade. The numbers of spectra measured for each component are sagebrush 69 (28), rabbitbrush 43 (15), greasewood 45 (16), shadscale 40 (8), halogeton 40 (8), saltbush 11 (5), grass 19 (5), soil 108 (35), stem 74 (27), and shade 60 (28). Numbers inside the parentheses are the numbers of spectra after averaging at each site. Each raw spectrum was examined and discarded if the spectrum included noise. The 252-band raw data were calibrated to reflectance using the reference panel measurements taken prior to scanning each data set and were convolved with a TM bandpass filter. The TM bandpass spectra of each component were averaged to obtain a representative spectrum for each component. The ten average reference spectra of surface components are presented in Figure 5.

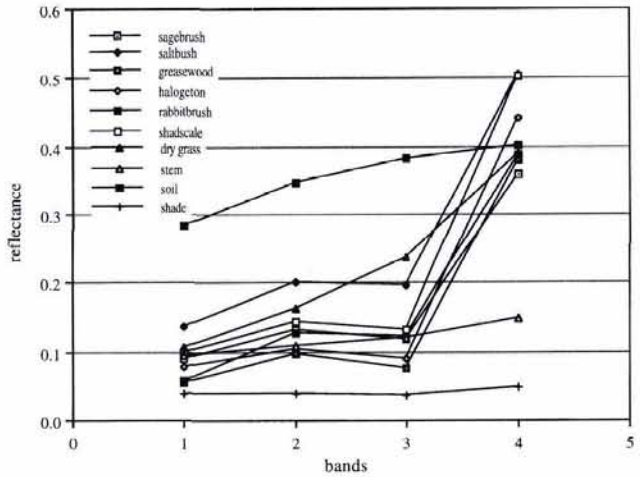

Figure 5. Reference spectra of major surface components.

Calibration of TM Data

The digital numbers of the TM image data were converted to reflectance data using the formulation presented in Markham and Barker (1985). Markham and Barker's (1985) reflectance conversion model was based on the assumption of a uniform Lambertian surface. This conversion needed to be done for combination of the data from two different sensors having different calibration, the TM multispectral scanner in Landsat 4 and the SE590 field spectrometer. The digital numbers of four TM bands (0.45 to 0.90 μm) data were converted to reflectance in three steps: (1) haze correction, (2) radiometric conversion, and (3) reflectance conversion. Haze correction is done using the improved dark-object subtraction technique by Chavez (1988). Chavez's haze correction model is an improvement to existing dark object subtraction methods and requires no outside information. Once haze effect is removed from the digital image data, the conversion from digital numbers to radiance, then to ground reflectance was done using the model reported by Robinove (1982) and Markham and Barker (1986).

Formulating a Mixture Model

Based on the results of the field estimates of surface components and the field spectra measurements of surface components in the study area, ten distinct surface components were identified: sagebrush, rabbitbrush, greasewood, shadscale, saltbush, halogeton, grass, woody materials, soil, and shade. The estimated average percent cover of surface components for the study area suggests that the soil (about 50 to 60 percent), vegetation (15 to 38 percent), and woody materials (2 to 33 percent) are the major surface components besides the shade component. The average percent cover of dry grass ranges from about 1.5 to 2.0 percent. Color of soil in the study area can be categorized into three groups: dark, intermediate, and light. Surface texture of the dark and intermediate color soil was mostly bumpy. The surface of light color soil was mostly cracked. Also, dark gray, dark reddish brown, and dark gravels were found on the surface. Most gravels found in the study area were less than 6 mm in diameter. The measured soil spectra reflects this variance: light soil shows high reflectance, intermediate color soil shows medium range reflectance, and dark soil shows low reflectance.

Based on these observations, spectral angles between soil spectra were calculated and compared to the signal-to-noise ratio to determine if light, intermediate brightness, and dark soil can be separated spectrally. Barker *et al.* (1983) reported that the TM noise level is less than 1 DN value. The dark signal for the study area scene, which is 49 in DN value, was decided by examining the minimum histogram value for TM bands 1, 2, 3, and 4. Accordingly, the signal-to-noise ratio of the study area image was adopted as 1/49 or 0.02041. The amount of error introduced in the estimates of the endmember fraction can be determined approximately by the signal-to-noise ratio times $1/\sin(\theta)$. When θ, the spectral angle in radians, is close to zero, $\sin(\theta)$ approaches θ. So when θ is 10 times larger than the signal-to-noise ratio, the endmember fractions can be estimated within the 10 percent error range, which is acceptable given that the underlying accuracy of the model using TM data is probably about 5 to 10 percent. This would mean that the column vectors (endmembers) can be decomposed to an accuracy of 10 percent when the column vectors are about 12 degrees (0.204 in radians) apart with 1/49 signal-to-noise ratio. All of the spectral angles between the light, intermediate, and dark soil spectra are less than 12 degrees. The largest angle is 8.6 degrees between the soil 10 and soil 3. This suggests that three different soil groups (light, intermediate, and dark) may not be separable but light and dark soils may be separable using only four TM bands data with a moderate error range. Finally, including the average soil, soil 3, and soil 10 spectra, 12 candidate endmembers were chosen to test the spectral separability. These include sagebrush, saltbush, greasewood, halogeton, rabbitbrush, shadscale, dry grass, stem, average soil, light soil, dark soil, and shade. The soil spectra and the reference spectra of the 12 endmembers used to calculate the angles are listed in Tables 2 and 3. The calculated spectral angles between the soils and between the 12 candidate endmembers are listed in Tables 4 and 5. According to the spectral angle analysis, with four TM bands, the two groups of vegetation—the vegetation with gray and hairy leaves such as sagebrush and saltbush, and the vegetation with green and/or shiny leaves such as greasewood, halogeton, and rabbitbrush—can be separated. Different types of vegetation in the same group may not be separable. Dry grass can be separated from the two groups of vegetation and soil. Dead stem can be separated from most of the candidate endmembers but may not be separated effectively from dark soil. The result of spectral angle analysis suggests that, with TM bands 1, 2, 3, and 4, the gray leaf vegetation, green leaf vegetation, dry grass, stem, soil, and shade components can be differentiated with 10 percent accuracy.

TABLE 2. REFERENCE SPECTRA OF SOILS USED FOR SPECTRAL ANGLE MEASUREMENT

Band	Soil Candidates									
	soil1	soil2	soil3	soil4	soil5	soil6	soil7	soil8	soil9	soil10
1	0.1820	0.1506	0.1376	0.2983	0.2092	0.2548	0.3019	0.3474	0.4043	0.4701
2	0.2403	0.1925	0.1801	0.3908	0.2848	0.3402	0.3615	0.4147	0.4790	0.5321
3	0.2827	0.2215	0.2088	0.4498	0.3358	0.3985	0.3895	0.4424	0.5021	0.5506
4	0.3203	0.2333	0.2500	0.4701	0.3661	0.4180	0.4064	0.4522	0.5053	0.5571

Soils 1,2,3: dark soils,
Soils 4,5,6,7: intermediate brightness soils,
Soils 8,9,10: light soils.

In this study, however, with only four spectral bands, a mixture model with three endmembers was chosen. The three endmembers are vegetation, soil, and shade. The shade component is a necessary component and should be included in a mixture for a reliable decomposition. With the average soil spectrum and the average shade spectrum, the average sagebrush spectrum was included as a representative of vegetation endmember because sagebrush was found at almost every sample site. A linear mixing model with four spectral bands and three endmembers is formulated as follows:

$$a_{11}x_1 + a_{12}x_2 + a_{13}x_3 + \varepsilon_1 = b_1$$
$$a_{21}x_1 + a_{22}x_2 + a_{23}x_3 + \varepsilon_2 = b_2$$
$$a_{31}x_1 + a_{32}x_2 + a_{33}x_3 + \varepsilon_3 = b_3$$
$$a_{41}x_1 + a_{42}x_2 + a_{43}x_3 + \varepsilon_4 = b_4$$

or

$$b_i = \sum_{j=1}^{3} a_{ij}x_j + \varepsilon_i, \qquad i = 1 \text{ to } 4 \tag{9}$$

where b_1 to b_4 are the TM image reflectance for bands 1 to 4 respectively; a_{11} to a_{41} are the reference spectrum of vegetation for bands 1 to 4; a_{12} to a_{42} are the reference spectrum of soil for bands 1 to 4; a_{13} to a_{43} are the reference spectrum of shade for bands 1 to 4; x_1 to x_3 are the unknown fractions for vegetation, soil, and shade respectively; and ε_1 to ε_4 are the error terms for each band. If all six TM bands data are used, at least one more endmember can be included in the mixture.

Unmixing in TM Data and Vegetation Fraction

The linear mixing model (Equation 9) can be expressed in error terms: i.e.,

$$\varepsilon_i = b_i - \sum_{j=1}^{3} (a_{ij}x_j), \qquad i = 1 \text{ to } 4.$$

The function to be minimized becomes

$$F = \varepsilon_1^2 + \varepsilon_2^2 + \varepsilon_3^2 + \varepsilon_4^2$$

or

$$F = \sum_{i=1}^{4} \varepsilon_i^2. \tag{10}$$

Now considering the first constraint, $x_1+x_2+x_3=1$ or $x_3=1-x_1-x_2$ and substituting $x_3=1-x_1-x_2$ into Equation 10, the function to be minimized becomes

$$F = c_1x_1^2 + c_2x_2^2 + c_3x_1x_2 + c_4x_1 + c_5x_2 + c_6$$

where the coefficients c_1 to c_6 are the functions of the endmember reflectance values (a_{ij}) and image pixel reflectance (b_i). To solve this problem, we need to find a minimum within the boundary, $0 \le x_1 \le 1$ and $0 \le x_2 \le 1$. The minimum of this function will occur when its partials are zero: i.e.,

$$\partial F/\partial x_1 = 2c_1x_1 + c_3x_2 + c_4 = 0$$
$$\partial F/\partial x_2 = 2c_2x_2 + c_3x_1 + c_5 = 0$$

Solving for x_1 and x_2:

$$x_1 = (c_3c_5 - 2c_2c_4)/(4c_1c_2 - c_3^2)$$
$$x_2 = (c_3c_4 - 2c_1c_5)/(4c_1c_2 - c_3^2)$$

According to the outcomes of the unconstrained x_1 and x_2 values, x_1 and x_2 are recalculated if necessary. The values of x_3 were determined accordingly.

The numerical method described in Shimabukuro (1987) was applied to unmix pixels in the TM image of the study area. A vegetation fraction image was produced by scaling the fraction values 0 to 255 (Figure 6). The vegetation fraction image was registered to UTM coordinates, and the calculated vegetation fractions of sample sites were compared with the field measurement (Figure 7). As shown in the Figure 7, the estimated range of the calculated vegetation fraction and field measurement corresponds quite well. The calculated vegetation fractions of the study area range from 0.24 to 0.38. The field measurements range from 0.18 to 0.37. It shows, however, a systematic distribution of errors. In areas of cluster 4, which has medium brightness soil color and medium size sagebrush mixed with greasewood, the vegetation was moderately well estimated. Vegetation was underestimated in the areas of clusters 1, 2, and 3 where soil color was dark. Vegetation was overestimated in the areas of clusters 5, 6, and 7 where soil color was very light. This result

TABLE 3. REFERENCE SPECTRA OF CANDIDATE ENDMEMBERS USED FOR SPECTRAL ANGLE MEASUREMENT

Band	Candidate Endmembers											
	1	2	3	4	5	6	7	8	9	10	11	12
1	0.08868	0.13590	0.05343	0.07888	0.05748	0.09955	0.10538	0.09375	0.28256	0.03758	0.1376	0.4701
2	0.13140	0.20118	0.09759	0.10350	0.12697	0.14406	0.16352	0.10950	0.34822	0.03807	0.1801	0.5321
3	0.11710	0.19616	0.07632	0.08956	0.12180	0.13112	0.23700	0.12081	0.38272	0.03639	0.2088	0.5506
4	0.35847	0.50658	0.38107	0.44064	0.38781	0.50366	0.38984	0.14783	0.40097	0.04615	0.2500	0.5571

1: sagebrush, 2: saltbush, 3: greasewood, 4: halogeton, 5: rabbitbrush, 6: shadscale, 7: dry grass, 8: stem, 9: soil, 10: shade, 11: soil3, 12: soil10.

TABLE 4. SPECTRAL ANGLES BETWEEN SOILS

Soil	cos(θ)	Angle in radians	Angle in degrees
soil2, soil1	0.99891	0.04675	2.67883
soil3, soil1	0.99973	0.02341	1.34130
soil3, soil2	0.99778	0.06662	3.81685
soil4, soil1	0.99894	0.04608	2.64012
soil4, soil2	0.99997	0.00827	0.47395
soil4, soil3	0.99774	0.06722	3.85163
soil5, soil1	0.99983	0.01817	1.04117
soil5, soil2	0.99925	0.03875	2.22044
soil5, soil3	0.99917	0.04083	2.33917
soil5, soil4	0.99938	0.03518	2.01548
soil6, soil1	0.99931	0.03714	2.12817
soil6, soil2	0.99980	0.01984	1.13694
soil6, soil3	0.99821	0.05990	3.43194
soil6, soil4	0.99990	0.01384	0.79278
soil6, soil5	0.99973	0.02313	1.32500
soil7, soil1	0.99567	0.09305	5.33153
soil7, soil2	0.99869	0.05118	2.93211
soil7, soil3	0.99425	0.10732	6.14924
soil7, soil4	0.99840	0.05662	3.24419
soil7, soil5	0.99606	0.08885	5.09051
soil7, soil6	0.99753	0.07033	4.02973
soil8, soil1	0.99441	0.10579	6.06142
soil8, soil2	0.99804	0.06256	3.58414
soil8, soil3	0.99275	0.12051	6.90461
soil8, soil4	0.99774	0.06728	3.85499
soil8, soil5	0.99494	0.10065	5.76684
soil8, soil6	0.99671	0.08110	4.64654
soil8, soil7	0.99991	0.01335	0.76464
soil9, soil1	0.99266	0.12120	6.94453
soil9, soil2	0.99698	0.07767	4.45034
soil9, soil3	0.99080	0.13575	7.77806
soil9, soil4	0.99664	0.08202	4.69928
soil9, soil5	0.99331	0.11577	6.63300
soil9, soil6	0.99541	0.09582	5.49030
soil9, soil7	0.99959	0.02863	1.64032
soil9, soil8	0.99988	0.01550	0.88823
soil10, soil1	0.99052	0.13783	7.89717
soil10, soil2	0.99540	0.09592	5.49590
soil10, soil3	0.98866	0.15074	8.63684
soil10, soil4	0.99490	0.10103	5.78855
soil10, soil5	0.99104	0.13398	7.67632
soil10, soil6	0.99342	0.11481	6.57799
soil10, soil7	0.99898	0.04517	2.58823
soil10, soil8	0.99942	0.03393	1.94431
soil10, soil9	0.99978	0.02117	1.21273

suggests that dark soil and light soil should be included as separate endmembers. The following are also possible causes that may contribute to some of the mismatches between the calculated vegetation fraction of the pixel in the image and the field measurement of corresponding sample point on the ground:

- Because of the limited number of spectral bands and the practical problem of solving an underdetermined system, it was not feasible to include more endmembers that could be differentiated. If green and gray vegetation, and light and dark soil were included as separate endmembers instead of the average soil as the representative of soil, and the average sagebrush spectra as the representative of all vegetation, the result of unmixing could have been improved;
- The decomposed fractions are density of greenness or biomass. On the other hand, the field measurements are the frequency of occurrence. The density and vigor of vegetation canopy were not considered in the field measurement; and
- locational errors are involved in locating sample sites on the map, in the image, and in the field, and also in registering the image to the UTM coordinates.

When greasewood was included as a vegetation endmember instead of sagebrush, vegetation was also underestimated in areas of clusters 1, 2, and 3, and moderately well estimated in areas of cluster 4. When darkest soil, most vigorous vegetation spectrum, and shade were used as endmembers for unmixing, vegetation was almost undetectable.

TABLE 5. SPECTRAL ANGLES BETWEEN CANDIDATE ENDMEMBERS

Candidate endmembers	cos(θ)	Angle in radians	Angle in degrees
sagebrush, saltbush	0.99854	0.05410	3.09984
greasewood, sagebrush	0.98628	0.16581	9.50026
greasewood, saltbush	0.97660	0.21673	12.41796
halogeton, sagebrush	0.98720	0.16015	9.17592
halogeton, saltbush	0.97775	0.21136	12.11028
halogeton, greasewood	0.99913	0.04173	2.39089
rabbitbrush, sagebrush	0.99588	0.09085	5.20541
rabbitbrush, saltbush	0.99224	0.12467	7.14304
rabbitbrush, greasewood	0.99325	0.11625	6.66053
rabbitbrush, halogeton	0.99163	0.12945	7.41677
shadscale, sagebrush	0.99567	0.09306	5.33168
shadscale, saltbush	0.98972	0.14349	8.22156
shadscale, greasewood	0.99700	0.07746	4.43831
shadscale, halogeton	0.99765	0.06856	3.92795
shadscale, rabbitbrush	0.99722	0.07464	4.27636
dry grass, sagebrush	0.97753	0.21241	12.17032
dry grass, saltbush	0.98672	0.16313	9.34677
dry grass, greasewood	0.93883	0.35157	20.14352
dry grass, halogeton	0.94003	0.34809	19.94384
dry grass, rabbitbrush	0.97064	0.24293	13.91881
dry grass, shadscale	0.96006	0.28357	16.24747
stem, sagebrush	0.91805	0.40765	23.35672
stem, saltbush	0.93687	0.35724	20.46807
stem, greasewood	0.84016	0.57321	32.84262
stem, halogeton	0.84557	0.56316	32.36694
stem, rabbitbrush	0.88850	0.47673	27.31474
stem, shadscale	0.87852	0.49804	28.53567
stem, dry grass	0.96122	0.27941	16.00917
average soil, sagebrush	0.88926	0.47508	27.21988
average soil, saltbush	0.91140	0.42411	24.29984
average soil, greasewood	0.80176	0.64056	36.70144
average soil, halogeton	0.80686	0.63198	36.20983
average soil, rabbitbrush	0.85700	0.54137	31.01836
average soil, shadscale	0.84398	0.56614	32.43734
average soil, dry grass	0.94377	0.33695	19.30579
average soil, stem	0.99747	0.07114	4.07578
shade, sagebrush	0.89634	0.45936	26.31922
shade, saltbush	0.91533	0.41446	23.74675
shade, greasewood	0.81201	0.62320	35.70692
shade, halogeton	0.81986	0.60963	34.92921
shade, rabbitbrush	0.85867	0.53813	30.83263
shade, shadscale	0.85339	0.54835	31.41805
shade, dry grass	0.93367	0.36627	20.98569
shade, stem	0.99469	0.10309	5.90681
shade, average soil	0.99375	0.11190	6.41160
dark soil, sagebrush	0.92365	0.39331	22.53503
dark soil, saltbush	0.94249	0.34080	19.52642
dark soil, greasewood	0.84862	0.55743	31.93825
dark soil, halogeton	0.85250	0.55004	31.51521
dark soil, rabbitbrush	0.89819	0.45515	26.07843
dark soil, shadscale	0.88543	0.48338	27.69564
dark soil, dry grass	0.96994	0.24582	14.08420
dark soil, stem	0.99868	0.05144	2.94750
dark soil, average soil	0.99583	0.09132	5.23237
dark soil, shade	0.98818	0.15388	8.81670
light soil, sagebrush	0.86893	0.51776	29.66571
light soil, saltbush	0.89208	0.46887	26.86446
light soil, greasewood	0.77535	0.68352	39.16288
light soil, halogeton	0.78191	0.67307	38.56391
light soil, rabbit brush	0.83139	0.58919	33.75813
light soil, shadscale	0.82036	0.60875	34.87889
light soil, dry grass	0.92349	0.39371	22.55767
light soil, stem	0.99330	0.11579	6.63445
light soil, average soil	0.99796	0.06382	3.65634
light soil, shade	0.99588	0.09076	5.20029
light soil, dark soil	0.98866	0.15074	8.63684

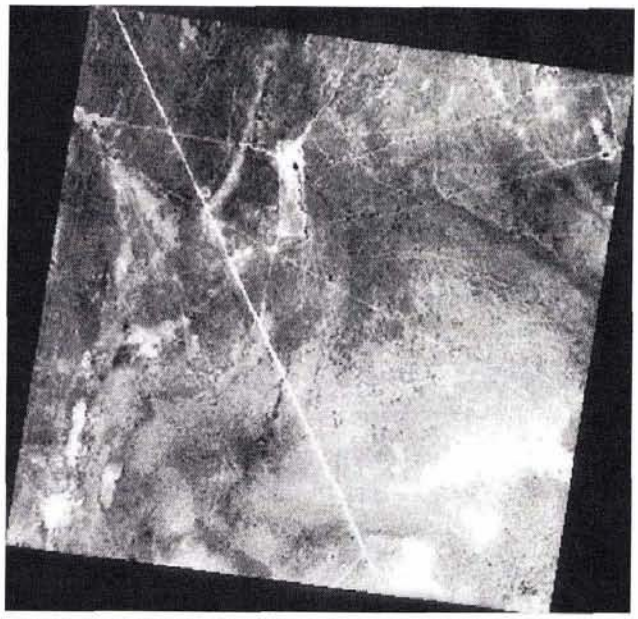

Figure 6. Vegetation fraction of the study area, Long Valley, Nevada. With sagebrush spectrum as a vegetation endmember. Calculated vegetation fractions range from 0.24 to 0.38. The image is produced by scaling the fraction values 0 to 255. Dark tone is less and brighter tone is more vegetation.

Conclusions

To explore the applicability of the inversion method, the discussion was focused on the theoretical and technical issues involved in this unmixing technique. The discussion in this study suggests that solving the minimum on the boundary condition is not necessarily the source of ambiguity in physical inversion problems. As discussed in the previous sections, even though it was not possible to formulate a complete mixture model due to the data and limitations in solving underdetermined systems, we have tested Shimabukuro and Smith's constrained least-squares method and discussed some important theoretical and technical issues involved. The results of the study suggest that, as long as a model is well conditioned, and with more spectral bands, the constrained least-squares method will provide the estimates of component fraction with a moderate error range. The algorithm adopted for solving least-squares problems with an inequality constraint is reasonable.

A method for testing the separability of candidate endmembers by calculating the angle of $\cos\theta$ between column vectors was presented in this study for the first time. This method provides a way to formulate a well-conditioned model for unmixing. This method also provides an idea about how many and what kind of components can be differentiated using a certain number of bands. For example, in spite of the popular belief that dry grass and soil have a similar spectral response pattern, and cannot be easily distinguished, the wide spectral angle (degree) between soil and dry grass suggests that their spectral pattern is not similar even with only four spectral bands. Using the method developed in this study for spectral angle measurement between candidate endmembers, we can measure the separability of candidate endmembers quantitatively and derive spectral endmembers objectively instead of choosing them arbitrarily. Also, the amount of error introduced in estimates of decomposed endmember fractions can be measured by comparing the spectral angles between endmembers and the signal-to-noise ratio.

Unmixing results suggest that it is important to include at least distinct scene components for reliable estimates of component fraction. As many studies have suggested, especially in arid rangeland where background soil is an important factor, at least dark and light soil should be included as separate endmembers unless soil has a uniform brightness over the entire study area. The following are the implications of unmixing experiments:

- The unmixing techniques can give moderate estimates of vegetation fractions in arid rangeland, even with four TM bands if the background soil shows a uniform brightness. A study area with light and dark soils can be partitioned into several regions that have a uniform soil background, and can be unmixed. If we use high spectral resolution data, such as AVIRIS, with improved field spectrometer, very low density vegetation (below 10 percent) may be mapped. Also, at least green-leaf vegetation and gray-leaf vegetation can be mapped as separate groups.
- The degree of spectral "pureness" of endmembers should be consistent between endmember spectra that are used for unmixing. If an average reference spectrum is used for one endmember, then the average reference spectra should be used for all the other endmembers in the study area. Also, if a spectrum of "pure" green leaves (totally separated from twigs and branches) is provided as an endmember, then the spectrum of twigs or branches should be provided also as a separate endmember at the same time to obtain reliable estimates of component fractions.

Spectral angle analysis strongly implies that, with high spectral resolution data, it may be possible to formulate a mixture with more endmembers than many studies suggest. So far, most studies distinguished only three or four endmembers with high spectral resolution data, such as AVIRIS. Recently, Boardman (1991), with AVIRIS data, formulated a seven-endmember linear mixture model for sedimentary facies analysis and used an unmixing procedure to map and remove the partial masking effects of the vegetation and soil components. With high spectral resolution image data, and with an improved field spectrometer, the inversion techniques will provide good methods for mapping sparse vege-

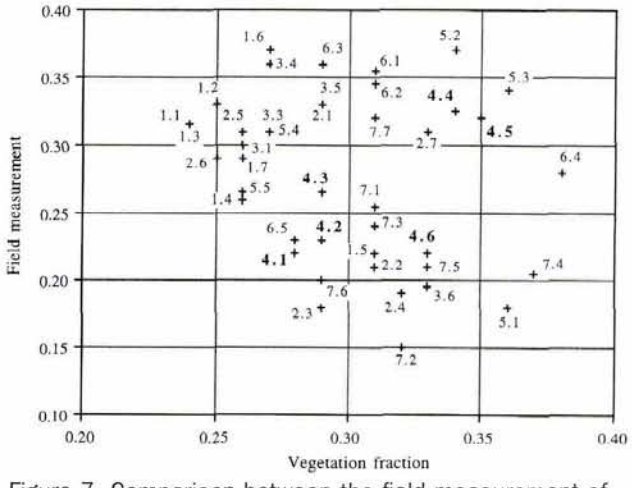

Figure 7. Comparison between the field measurement of vegetation cover and the calculated vegetation fraction. With sagebrush spectrum as a vegetation endmember. For each sample site, the first digit represents the cluster number. Following the decimal represents the number of sample site for each cluster.

tation and information extraction for various geographic applications. According to the results of this paper and the experiments of this study, it seems that the ambiguity (uncertainty) problem in the physical inversion problems arises from the inability to provide a complete set of representative reference spectra and to formulate a well-conditioned spectral mixture, not from the least squares-method itself.

References

Adams, J.B., M.O. Smith, and P.E. Johnson, 1986. Spectral mixture modeling: A new analysis of rock and soil types at the Lander 1 site, *Journal of Geophysical Research*, 91(B8):8098–8112.

Bammel, B.H., and R.W. Birnie, 1994. Spectral reflectance response of big sagebrush to hydrocarbon-induced stress in the Bighorn Basin, Wyoming, *Photogrammetric Engineering & Remote Sensing*, 60(1):87–96.

Barker, J.L., R.B. Abrams, D.L. Ball, and K.C. Leung, 1983. Characterization of radiometric calibration of Landsat-4 TM reflective bands, *Proceedings of the Landsat 4 Science Characterization Early Results Symposium*, Vol. II, Thematic Mapper(TM), Part I, NASA, pp. 373–474.

Boardman, J.W., 1989. Inversion of imaging spectrometry data using singular value decomposition, *Proceedings of International Geoscience and Remote Sensing Symposium*, pp. 2069–2072.

———, 1991. *Sedimentary Facies Analysis Using Imaging Spectrometry: A Geophysical Inverse Problem*, Ph.D. dissertation. Department of Geological Sciences, University of Colorado, Boulder, Colorado.

Chavez, P.S., Jr., 1988. An improved dark-object subtraction technique for atmospheric scattering correction of multispectral data, *Remote Sensing of Environment*, 24:459–479.

Eakin, T.E., 1961. Ground water appraisal of Long Valley, White Pine and Elko Counties, Nevada, *USGS Ground Water Resources-Reconnaissance Series*, Report 3.

Huete, A.R., 1986. Separation of soil-plant spectral mixtures by factor analysis, *Remote Sensing of Environment*, 19:237–251.

Markham, B.L., and J.L. Barker, 1985. Spectral characterization of the Landsat Thematic Mapper sensor, *International Journal of Remote Sensing*, 6(5):697–716.

———, 1986. Landsat MSS and TM post-calibration dynamic ranges, exoatmospheric reflectances and at-satellite temperatures, *Landsat Technical Notes*, EOSAT.

McCoy, R.M., L.F. Scott, and P.J. Hardin, 1989. The spectral response of sagebrush in areas of hydrocarbon production, *Proceedings of the Seventh Thematic Conference on Remote Sensing for Exploration Geology*, Calgary, Alberta, Canada, 2: 751–755.

Milton, E.J., 1987. Principles of field spectroscopy, *International Journal of Remote Sensing*, 8(12):1807–1827.

Pace, W.H., and D.M. Detchmendy, 1973. A fast algorithm for the decomposing of multispectral data into mixtures, *Remote Sensing of Earth Resources*, 2:831–848.

Pech, R.P., A.W. Davis, R.R. Lamacraft, and R.D. Graetz, 1986. Calibration of Landsat data for sparsely vegetated semi-arid rangelands, *International Journal of Remote Sensing*, 7(12):1729–1750.

Roberts, D.A., 1991. *Separating Spectral Mixtures of Vegetation and Soils*, Ph.D. dissertation, University of Washington.

Roberts, D.A., M.O. Smith, and J.B. Adams, 1993. Green vegetation, nonphotosynthetic vegetation, and soils in AVIRIS data, *Remote Sensing of Environment*, 44:255–269.

Robinove, C.J., 1982. Computation with physical values from Landsat Digital Data, *Photogrammetric Engineering & Remote Sensing*, 48(5):781–784.

Shimabukuro, Y.E., 1987. *Shade Images Derived from Linear Mixing Models of Multispectral Measurements of Forested Areas*, Ph.D. dissertation, Colorado State University.

Shimabukuro, Y.E., and J.A. Smith, 1991. The least-squares mixing models to generate fraction images derived from remote sensing multispectral data, *IEEE Transactions on Geoscience and Remote Sensing*, 29(1):16–20.

Smith, M.O., P.E. Johnson, and J.B. Adams, 1985. Quantitative determination of mineral types and abundances from reflectance spectra using principal components analysis, *Proceedings of the 5th Lunar and Planetary Science Conference, Part 2, Journal of Geophysical Research*, Vol. 90, Supplement, pp. c797–c804.

Smith, M.O., S.L. Ustin, J.B. Adams, and A.R. Gillespie, 1990. Vegetation in desert: I. A regional measure of abundance from multispectral image, *Remote Sensing of Environment*, 31:1–26.

Strang, G., 1980. *Linear algebra and its applications*, Second Edition, Academic Press, New York.

Twomey, S., 1977. *Introduction to the Mathematics of Inversion in Remote Sensing and Indirect Measurements*, Elsevier Scientific Publishing Company, Amsterdam, The Netherlands.

(Received 5 February 1996; accepted 5 November 1996; revised 9 December 1996)